Challenges and opportunities of near and mid-infrared photonics based on SiGe and Ge

M. Takenaka[a,b], Y. Kim[a], J. Han[a,b], J. Kang[a,b], and S. Takagi[a,b]

[a] Department of Electrical Engineering and Information Systems, The University of Tokyo, Bunkyo-ku, Tokyo 113-8656, Japan
[b] JST- CREST, Chiyoda-ku, Tokyo 102-0076, Japan

Silicon-germanium (SiGe) and germanium (Ge) have been investigated as high-mobility channel materials for high-performance metal-oxide-semiconductor field-effect transistors (MOSFETs). The intense development of heterogeneous integration of SiGe and Ge on Si has given us opportunities to extend functionalities of photonic integrated circuits based on Si photonics technologies. We have investigated strain engineering by SiGe for enhancing modulation efficiency in Si optical modulators. By using the light hole effective mass in strained SiGe, we have demonstrated the enhanced plasma dispersion effect in SiGe. In addition to low-dark-current Ge photodetectors with GeO_2 passivation, we have proposed Ge CMOS photonics for mid-infrared integrated photonics platform. We have successfully demonstrated Ge passive waveguide devices as well as carrier-injection variable optical attenuator operated at a 2-μm wavelength on Ge-on-Insulator wafer.

Introduction

High-mobility semiconductor-based metal-oxide semiconductor field-effect transistors (MOSFETs) are one of the enabling technologies to sustain the Moore's law in the coming post-scaling era [1,2]. Silicon-germanium (SiGe) and germanium (Ge) have been investigated as high-mobility channel materials for high-performance metal-oxide-semiconductor field-effect transistors (MOSFETs). The intense development of heterogeneous integration of SiGe and Ge on Si has given us opportunities to integrate new functionalities on Si platform. Fig. 1 shows bandgap energy in SiGe and GeSn alloys. When the Ge content in SiGe increases, the bandgap energy covers the near-infrared (NIR) wavelength range used in the optical fiber communication system. Thus, we are able to monolithically integrated SiGe/Ge-based photodetectors (PDs) on Si platform, evoking the emergence of Si photonics technology as a standard photonics integrated circuit (PIC) platform [3]. Moreover, Ge-based lasers [4,5] and electro-absorption optical modulators [6] have been reported by using the unique bandgap property of Ge. GeSn has also been significantly studied for photonics application. Since the bandgap of GeSn shrinks further when the Sn content increases, GeSn PDs enable extending the detectable wavelength range toward the mid-infrared (MIR) regime [7]. When the Sn content in GeSn exceeds approximately 10%, GeSn becomes a direct-gap semiconductor, enabling GeSn lasers as reported recently [8]. Thus, the heterogeneous integration of IV-group alloys on Si allows us to extend functionalities of photonic integrated circuits (PICs) based on the Si photonics

technology for near-infrared optical communication and mid-infrared bio/medical sensing applications.

We have investigated the heterogeneous integration of SiGe and Ge on Si for integrated photonics through CMOS compatible process. We have studied the strain engineering technology based on SiGe for enhancing a modulation efficiency of Si-based optical modulators. In addition to Ge photodetector (PD), we have proposed a novel Ge PIC platform on Ge-on-Insulator (GeOI) wafer for MIR wavelength. In this paper, we present our recent progresses in PICs based on SiGe and Ge to discuss challenges and opportunities of SiGe and Ge for near and mid-infrared integrated photonics.

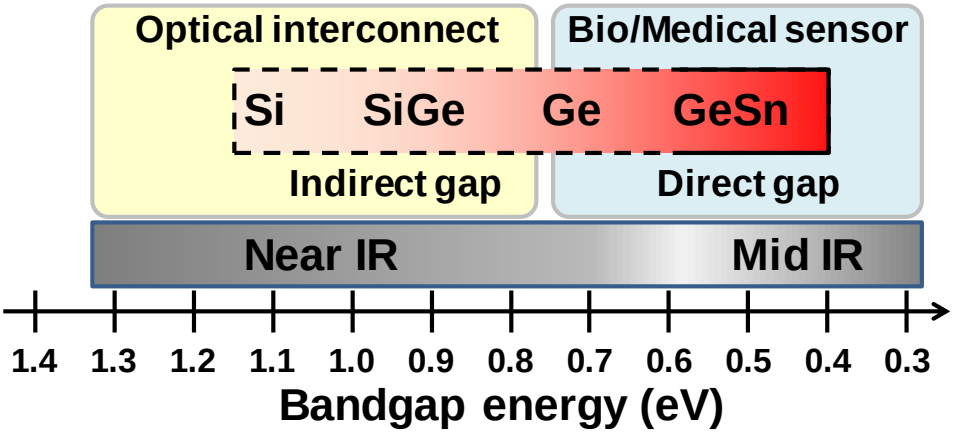

Figure 1. Bandgap energy in SiGe and GeSn alloys, which covers from near-infrared and mid-infrared wavelength ranges.

Strain Engineering based on SiGe for optical modulators

Among Si photonic components, Si-based optical modulators are one of the key building blocks for high-performance and low-power optical interconnection especially in datacenter networks. Since there is no significant electric-optic effect in Si, the free-carrier effects such as the plasma dispersion effect and free-carrier absorption are the most common methods to modulate optical signal. Fig. 2 summarizes the carrier modulation scheme in Si optical modulators [9]. Basically we have three modulation schemes: accumulation, injection, and depletion. Accumulation based on an MOS capacitor shown in Fig. 2(a) provides us the most efficient optical modulation in conjunction with equivalent oxide thickness (EOT) scaling. However, a large capacitance in the MOS structure limits the modulation speed; thus, there is the trade-off relationship between modulation efficiency and modulation speed. In addition, a waveguide mesa on the gate oxide should be formed by poly Si, making the fabrication procedure a bit complicated. The doped poly Si waveguide also causes a large propagation loss. A carrier-injection optical modulator based on a forward-biased PIN junction shown in Fig. 2(b) enables high modulation efficiency. However, the minority carrier lifetime limits the modulation speed to a few-hundred MHz. Although the pre-emphasis driving scheme can boost the modulation speed up to 50 GHz, an increase in the power consumption is unavoidable. In terms of the balance between modulation efficiency and speed, a carrier-depletion scheme based on a reverse-

biased PN junction shown in Fig. 2(c) is adopted in most of Si optical modulators reported so far.

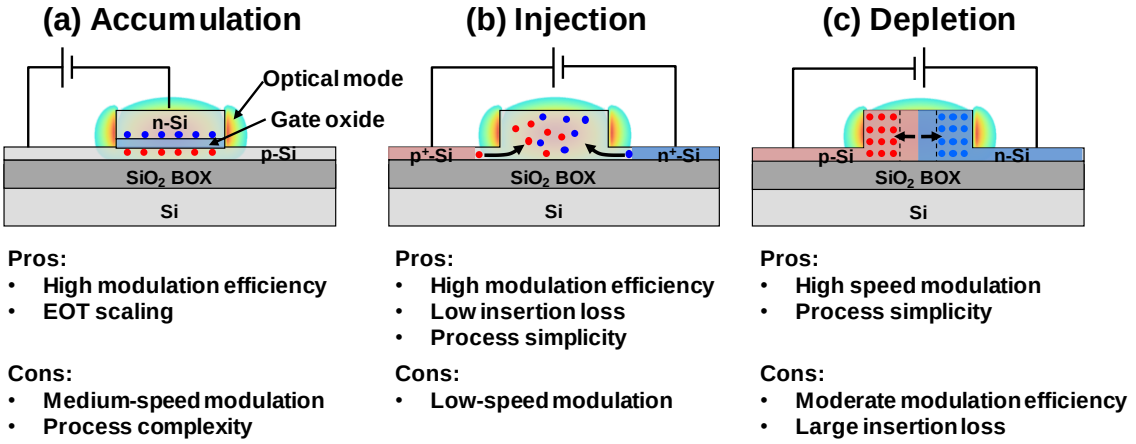

Figure 2. Carrier modulation schemes for Si-based optical modulators: (a) accumulation, (b) injection, and (c) depletion.

One of the figure-of-merit for optical modulators is $V_\pi L$, a driving voltage for π phase shift multiplied by a device length, which expresses modulation efficiency. By taking into account the plasma dispersion effect in Si for near-infrared wavelengths [10], a typical $V_\pi L$ in depletion-based Si optical modulator is 1 Vcm to 4 Vcm, resulting in a large device length. Hence, it is quite important to improve $V_\pi L$ for Si-based optical modulators. According to the Drude model, the plasma dispersion effect and free-carrier effect are expressed as follows:

$$\Delta n = -\left(e^2\lambda^2/8\pi^2c^2\varepsilon_0 n\right)\left[\Delta N_e/m^*_{ce} + \Delta N_h/m^*_{ch}\right] \quad (1)$$

$$\Delta\alpha = -\left(e^3\lambda^2/4\pi^2c^3\varepsilon_0 n\right)\left[\Delta N_e/m^{*\,2}_{ce}\mu_e + \Delta N_h/m^{*\,2}_{ch}\mu_h\right] \quad (2)$$

where Δn is refractive index change, $\Delta\alpha$ is absorption change, ΔN_e is free electron density change, ΔN_h is free hole electron density, e is the elementary charge, ε_0 is the permittivity in vacuum, c is the speed of light in vacuum, λ is the wavelength, n is the unperturbed refractive index, m^*_{ce} is the conductivity effective mass of electrons, m^*_{ch} is the conductivity effective mass of holes, μ_e is the electron mobility, and μ_h is the hole mobility. From equations (1) and (2), the refractive index change and absorption change due to the free-carrier effects is enhanced if the effective electron and hole masses are decreased. Thus, we have proposed the strain engineering for enhancing the free-carrier effects through effective mass modulation.

To obtain a light effective mass in electron or hole, we have proposed to use strained SiGe as a waveguide material [11]. When a SiGe layer is grown on Si, compress strain is applied into the SiGe film, resulting in the light hole effective mass as is well known. Fig. 3(a) shows the hole effective mass in strained SiGe as a function of the Ge fraction calculated by the k·p method. When the Ge fraction is more than 0.5, the hole effective

mass is reduced by 1/3. From this result, we have predicted the enhancement factor in Δn and $\Delta \alpha$ as shown in Figs. 3 (b) and (c). It is expected that we can achieve more than 3 times greater enhancements in both refractive index change and absorption change when the Ge fraction is 0.5.

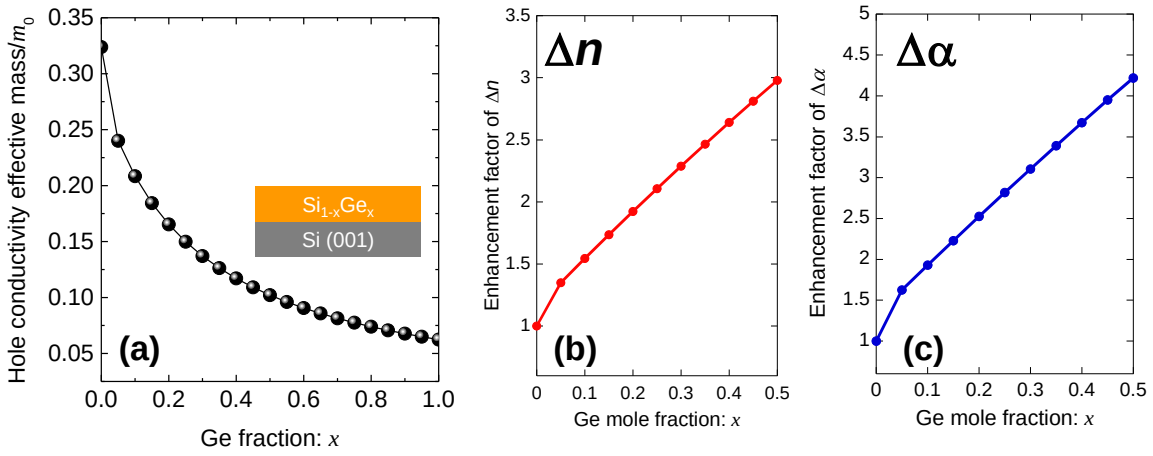

Figure 3. (a) Hole effective mass in SiGe, enhancement factors in (b) refractive index change, and (c) absorption change as a function of Ge fraction in SiGe [11].

To explore the enhanced free-carrier effects in strained SiGe, we have examined a carrier-injection SiGe optical modulation as shown in Fig. 4(a) [12]. A strained SiGe layer is embedded in a Si waveguide mesa. When free carriers are injected into the waveguide mesa through a lateral PIN junction, electrons and holes are accumulated in the SiGe layer, contributing the refractive index and absorption modulation. Fig. 4(b) is the fabrication procedure. First we grow a SiGe layer and a Si cap on a silicon-on-insulator (SOI) wafer by CVD. After forming the waveguide mesa by dry etching, the lateral PIN junction is formed by ion implantation and activation annealing. We perform SiO_2 passivation and form Al electrodes.

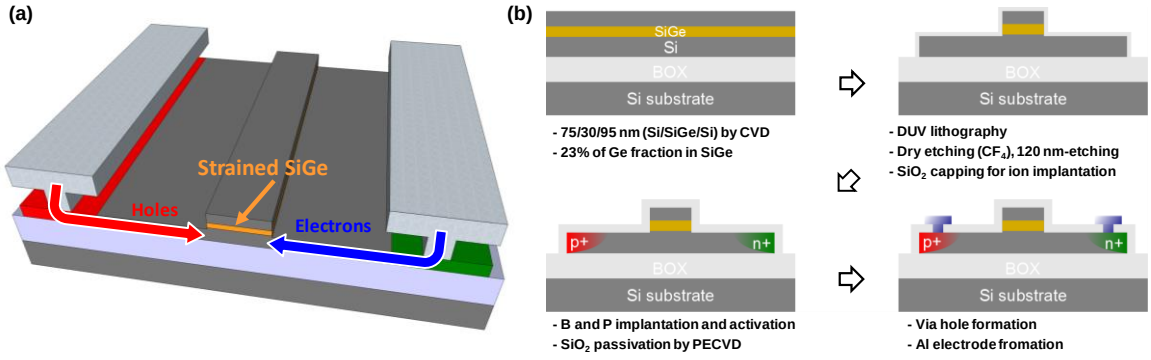

Figure 4. (a) schematic of carrier-injection SiGe optical modulator and (b) fabrication procedure [12].

Fig. 5(a) shows a cross-section TEM image of the SiGe waveguide after dry etching. A 30-nm-thick $Si_{0.77}Ge_{0.23}$ layer was allocated at the center of the 600-nm-wide waveguide core to maximize the overlap between free carriers and the optical mode. A top-view of the fabricated device is shown in Fig. 5(b). The lateral PIN junction is formed along the SiGe waveguide to inject free carriers into the waveguide. A continuous-wave light at a 1550 nm wavelength is injected into the waveguide from the cleaved edge and an output power is measured by an InGaAs optical power meter to evaluate the absorption modulation by the free-carrier absorption. Fig. 5(c) shows the measured attenuation changes with varied injection current in the SiGe (red dots) and Si control (black dots) devices. A shown in Fig. 5(c), we find the significantly greater absorption modulation in the SiGe device than in the Si device. The injection current for 20-dB attenuation in the SiGe device is 24 mA/mm which is approximately half of that in the Si. The numerical simulation results shown as the solid lines in Fig. 5(c), which take into account the enhanced free-carrier effects in SiGe, are in good agreement with the experimental results. Therefore, we can conclude that the free-carrier absorption is enhanced in strained SiGe owing to its light hole effective mass. By optimizing the distance between the junction edge to the waveguide edge, the record-high absorption modulation efficiency is obtained by using the SiGe strain engineering [13].

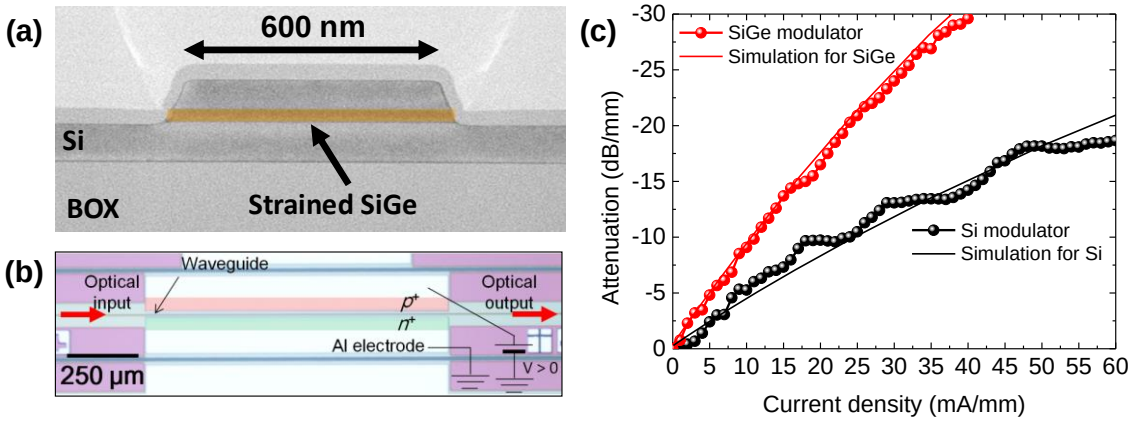

Figure 5. (a) cross-sectional TEM of SiGe embedded waveguide, (b) top-view of the SiGe optical modulator, and (c) absorption modulation characteristics of SiGe and Si control devise [12].

We have also explored the enhanced plasma dispersion effect in strained SiGe [14]. To evaluate phase change in the SiGe waveguide precisely, an asymmetric Mach-Zehnder interferometer (MZI) is formed as shown in Fig. 6(a). By measuring the resonance wavelength peak shift, the phase shift value can be deduced. Fig. 6(b) shows the measured phase shift in the SiGe and Si MZI optical modulators as the injection current increases. It is found that the SiGe device exhibits greater phase shift than the Si device, which is the evidence of the enhanced plasma dispersion effect in strained SiGe. Thus, we have successfully demonstrated that the strain engineering by SiGe is quite effective to enhance the modulation efficiency of Si-based optical modulators. A clear eye opening at 10-Gbps modulation is also achieved by using a pre-emphasis driving scheme as shown in the inset of Fig. 6(b). Since SiGe has been widely used in the standard CMOS process as channel and source/drain materials, the presented SiGe strain engineering for Si-based optical modulators possesses excellent CMOS compatibility.

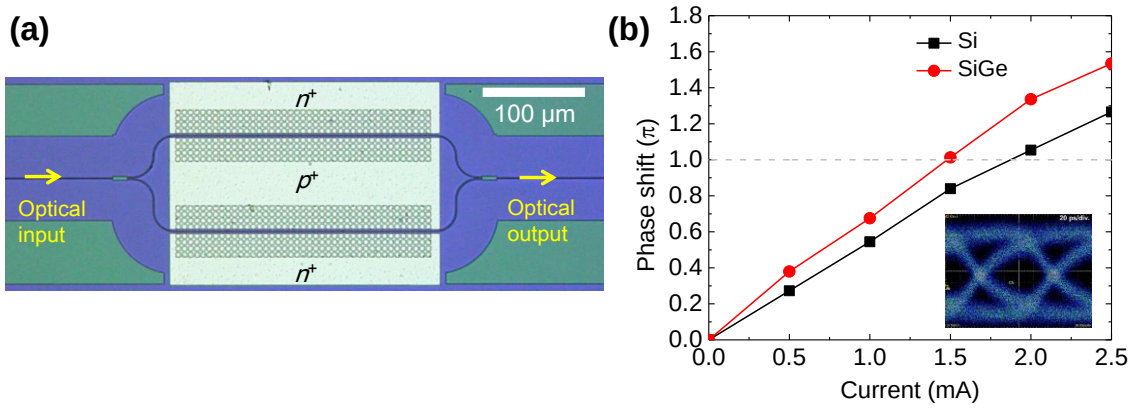

Figure 6. (a) top-view of asymmetric Mach-Zehnder interferometer SiGe optical modulator and (b) measured phase shift in SiGe and Si control devises [14].

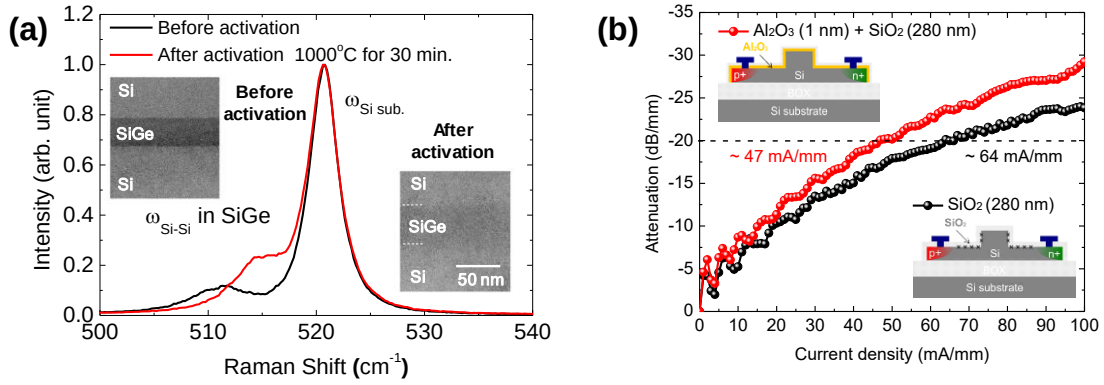

Figure 7. (a) Raman spectra and TEM images of the SiGe layer before and after activation annealing and (b) attenuation characteristics in Si optical modulators with Al_2O_3 and SiO_2 passivation as a function of injection current [15].

One of the major challenges in the fabrication of the carrier-injection SiGe optical modulators is the diffusion of Ge atoms in the SiGe layer during the activation annealing. We perform the activation annealing at 1000 °C for 30 min after depositing the SiO_2 layer by PECVD to passivate the Si surface simultaneously. The surface passivation is especially important for carrier-injection optical modulators to achieve high injection efficiency. However, the high-temperature annealing causes the Ge out-diffusion from the SiGe layer into the Si layers [12]. Fig. 7(a) shows Raman spectra of the SiGe layer before and after the activation annealing. The Raman spectroscopy indicates the Ge content decreases after the annealing, which is also confirmed in the TEM image as shown in the inset of Fig. 7(a). It is found from Fig. 7(a) that the Ge content decrease from 23% to 14%, which degrades the enhancement in the modulation efficiency originated from the SiGe layer. Thus, it is important to introduce short-time annealing such as flash lamp annealing or laser annealing for suppressing the Ge diffusion. It is also important to obtain well-passivated Si surfaces with a low-temperature process. We find that an Al_2O_3 layer deposited by ALD is effective to passivate the device [15]. Fig. 7(b) shows the absorption modulation characteristics in Si optical modulators which are passivated by ALD Al_2O_3 or PECVD SiO_2. We only apply

the high-temperature annealing to the device with PECVD SiO_2 passivation. As shown in Fig. 7(b), the Al_2O_3 passivation formed at 200 °C is superior to the PECVD SiO_2 passivation in terms of the absorption modulation efficiency, which is comparable to the thermally grown SiO_2 passivation. Hence, there is plenty of room for improving the modulation efficiency in the carrier-injection SiGe optical modulators by introduction the short-time annealing and Al_2O_3 passivation simultaneously.

We have also examined a depletion-based SiGe optical modulator. To take full advantage of the enhanced free-carrier effects in SiGe, a vertically formed PN junction in a waveguide mesa is considered. Fig. 8(a) shows a schematic of depletion-based SiGe optical modulator in which the p^+-SiGe layer is depleted when a reverse bias voltage is applied, resulting in efficient optical modulation [16]. The numerically analyzed modulation efficiency $V_\pi L$ as a function of applied reverse voltage is shown in Fig. 8(b). As the Ge content increase, $V_\pi L$ decreases significantly owing to the enhanced plasma dispersion effect in SiGe. When the Ge content is 0.3, the $V_\pi L$ of 0.3 Vcm at -2 V bias voltage is predicted. Recently we have experimentally demonstrated the depletion-based SiGe optical modulator [17].

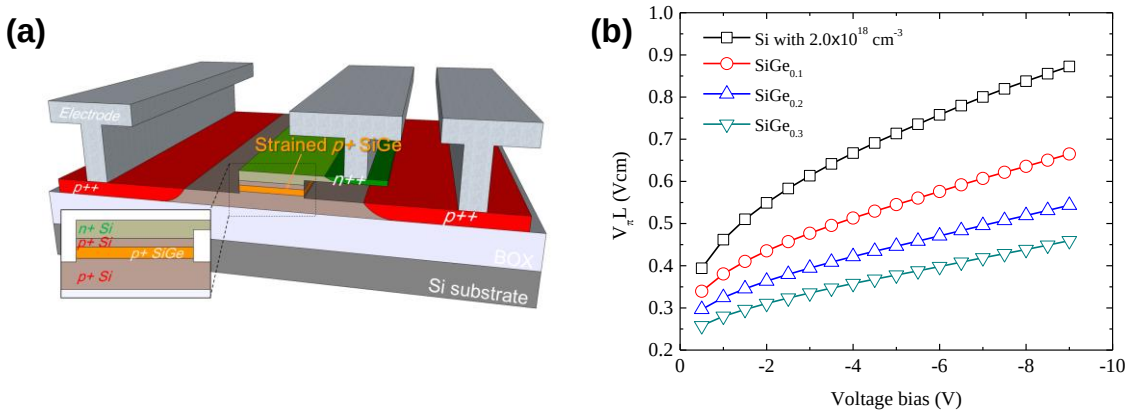

Figure 8. (a) schematic of depletion-based SiGe optical modulator and (b) numerically analyzed modulation efficiency in SiGe optical modulator with varied Ge contents [16].

An accumulation-based SiGe optical modulator is also considered as shown in Fig. 9(a) [11]. A p-SiGe quantum well (QW) is formed underneath a gate oxide. Since the accumulation layer is quite thin, the 3-nm-thick SiGe layer is sufficient to obtain hole-induced refractive index change in the SiGe layer, enabling the high Ge content SiGe growth. The quantum confinement in the SiGe QW also increase the bandgap energy, which can extend available wavelength range. For a 1550 nm wavelength, the Ge content up to 50% is acceptable in case of the SiGe QW. In conjunction with EOT scaling, we predict the $V_\pi L$ of 0.033 Vcm by using the $Si_{0.5}Ge_{0.5}$ QW. To achieve high modulation efficiency in the SiGe MOS optical modulator, the high-quality SiGe MOS interface is indispensable. It is well known that a conventional thermal oxidation is not effective for forming high-quality SiGe interfaces due to the Ge pile-up. Thus, we have investigated plasma post-nitridation for SiGe interfaces [18,19]. After depositing an Al_2O_3 layer on the SiGe surface by ALD, N_2 plasma is irradiated on the surface which forms a SiGe-ON

interfacial layer between the Al_2O_3 and SiGe. Fig. 9(b) is C-V curves of post-nitrided Al_2O_3/SiGe MOS capacitor. The well-behaved C-V characteristic with small frequency dispersion is obtained. The energy distribution of interface traps is evaluated by the conductance method as shown in Fig. 9(c). It is found that the interface trap density can be reduced by a factor of ten by the N_2 plasma irradiation. Thus, we are able to fabricate a high-performance SiGe MOS optical modulator by using plasma post-nitridation, which is also applicable to SiGe p-channel MOSFETs.

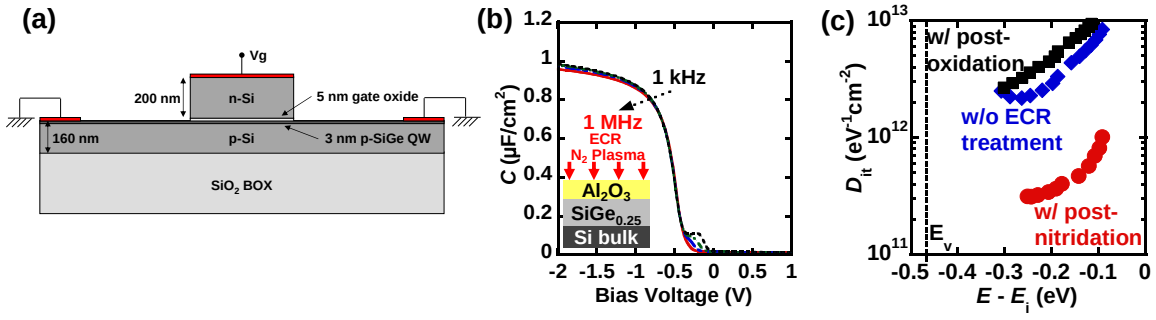

Figure 9. (a) schematic of accumulation-based SiGe optical modulator, (b) C-V curves of Al_2O_3/SiGe MOS capacitor with plasma post-nitridation, and (c) interface trap distributions in Al_2O_3/SiGe interfaces [11,18,19].

Ge photonics for near and mid-infrared wavelengths

Ge is now widely used as PDs for near-infrared wavelengths on Si photonics platform because its direct bandgap energy at the Γ point is approximately 0.8 eV. Considerable efforts of Ge crystal growth have make it possible to overcome the lattice-mismatch between Ge and Si, enabling monolithic integration of Ge PDs on Si. However, in the 2000s, large dark current in Ge PDs was one of the major technology issues. The physical origins of the dark current in Ge PDs was not clearly understood at that moment. Although crystal defects in a Ge layer grown on Si were considered to increase the dark current, we found that the n/p junction formation and surface passivation are critical for suppressing the dark current.

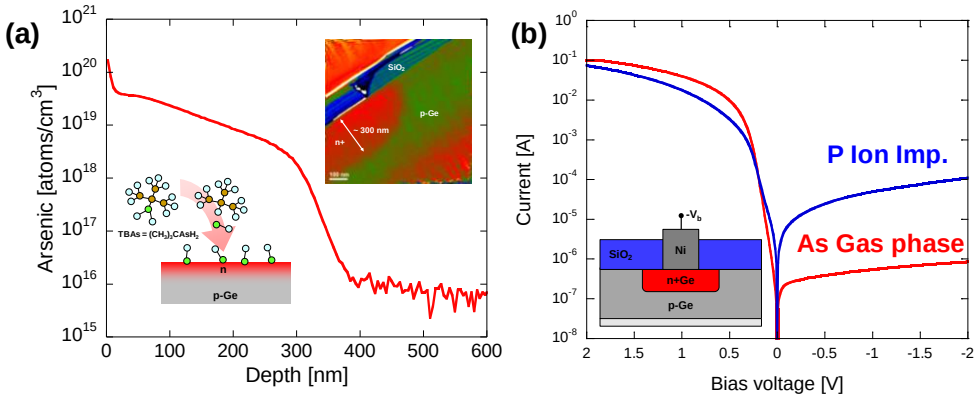

Figure 10. (a) Arsenic profile doped in Ge by using TBAs-based gas-phase doping and (b) I-V curves of n+/p junction formed by gas-phase doping and ion implantation [20,21].

We have found that one of the major origin of the dark current in Ge PDs is junction bulk leakage current. In most of Ge PDs, a n/p junction in a Ge mesa is formed by ion implantation of P or As. However, the abnormally fast diffusion of implanted P and As during activation annealing makes it quite difficult to form high-quality PN junctions. To overcome this obstacle, we have introduced a novel gas-phase doping based on tertiarybutylarsine (TBAs) [20]. When TBAs with hydrogen carrier gas is injected to a heated quartz tube where Ge samples are located, decomposed As atoms diffuse into Ge. Fig. 10 (a) shows the As profile doped in Ge through the TBAs-based gas-phase doping. The diffusion process from the gas source introduces no crystal damage, resulting in the formation of high-quality n^+/p junction. The comparison in I-V characteristics of n/p junctions formed by the gas-phase doping and P implantation is shown in Fig. 10(b). The gas-phase doped device exhibit a factor of 100 smaller dark current than the implanted device [21].

We have also revealed the importance of surface passivation for suppressing the dark current. Historically Ge surface passivation seems quite difficult as compared with Si. However, we have found that GeO_2 formed by high-temperature thermal oxidation passivate Ge surfaces very well [22]. Thus, we have applied the GeO_2 passivation to Ge PDs in conjunction with the gas-phase doped n/p junction as shown in Fig. 11(a) [21]. The I-V curve of the GeO_2 passivated Ge PD in Fig. 11(b) exhibits a high I_{on}/I_{off} ration near 10^7 and extremely small dark current density of 0.032 mA/cm^2. We have also found that the dark current depends on the gate bias, indicating the importance of the surface potential for low dark current operation. By controlling the surface potential by fixed charges in the Al_2O_3 and PECVD SiO_2 capping layers, we have revealed that the dark current can be suppressed when the Ge surface is in the accumulation condition [23]. Thus, we have successfully clarify the physical origins of the dark current and shown the way toward low-dark-current Ge PDs.

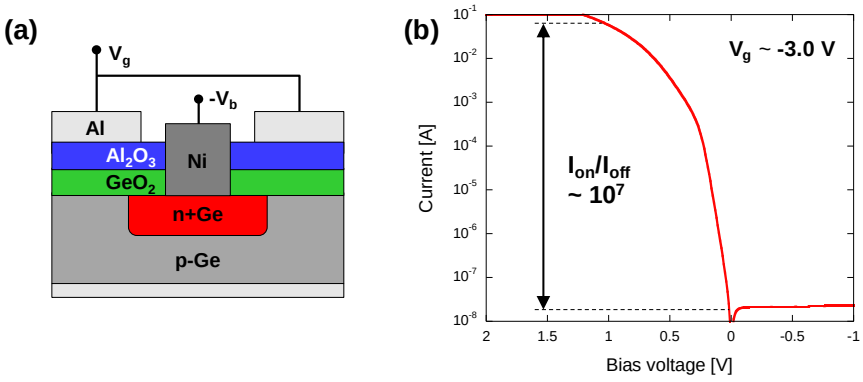

Figure 11. (a) Schematic and (b) I-V curve of GeO_2-passivated Ge PD with gas-phase doped junction [21].

Ge is recently going to gain much attention as a waveguide material for MIR integrated photonics [24,25]. MIR photonics has a great potential for bio/medical sensor application. Si photonics platform contributes the development of MIR photonic chips. However, Si is opaque when a wavelength is larger than 8 μm, limiting available MIR spectrum. On the

other hand, the transparent wavelength range of Ge covers the entire MIR spectrum. Thus, Ge is more suitable for MIR integrated photonics application. We have recently proposed the Ge CMOS photonics as shown in Fig. 12 [26]. Ge rib/strip waveguides, which are transparent for MIR wavelengths, can be fabricated on a GeOI wafer. The strong two dimensional optical confinement in the GeOI structure is a key enabler to build ultra-compact mid-infrared PICs as like Si photonics for near-infrared PICs. Moreover, we can monolithically integrated Ge-based CMOS electrical circuits which can outperform Si CMOS thanks to the high hole and electron mobility in Ge.

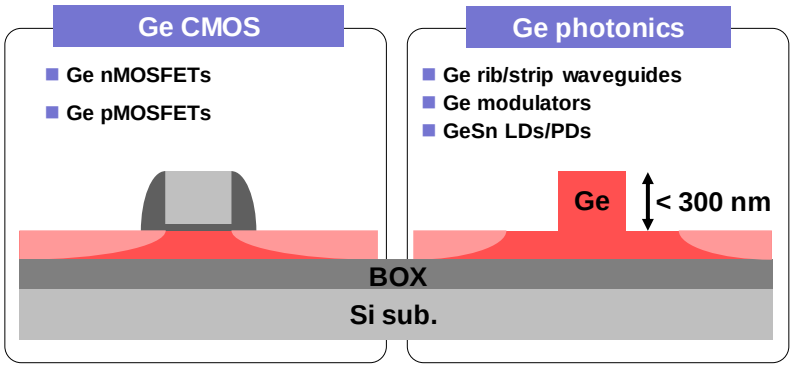

Figure 12. Concept of Ge CMOS photonics platform [26].

To realize the Ge CMOS photonics platform, we have fabricated a GeOI wafer by using wafer bonding and smart-cut^{TM} technologies [26]. Fig. 13(a) shows the fabrication procedure of the GeOI wafer. After H^+ ion implantation into a Ge bulk wafer, the Ge surface is passivated by ALD Al_2O_3 with plasma post-oxidation [27] to form a superior back interface after bonding. Then the Ge wafer is bonded on an SiO_2/Si wafer. A 2-μm-thick SiO_2 buried oxide (BOX) layer is prepared by wet thermal oxidation for the strong optical confinement in the Ge waveguide. After wafer bonding, the Ge wafer is split by thermal annealing. Finally, the Ge surface is planarized by CMP. A cross-section TEM of the GeOI wafer in Fig. 13(b) shows that a few-hundred-μm thick uniform Ge layer is well bonded on the SiO_2 BOX.

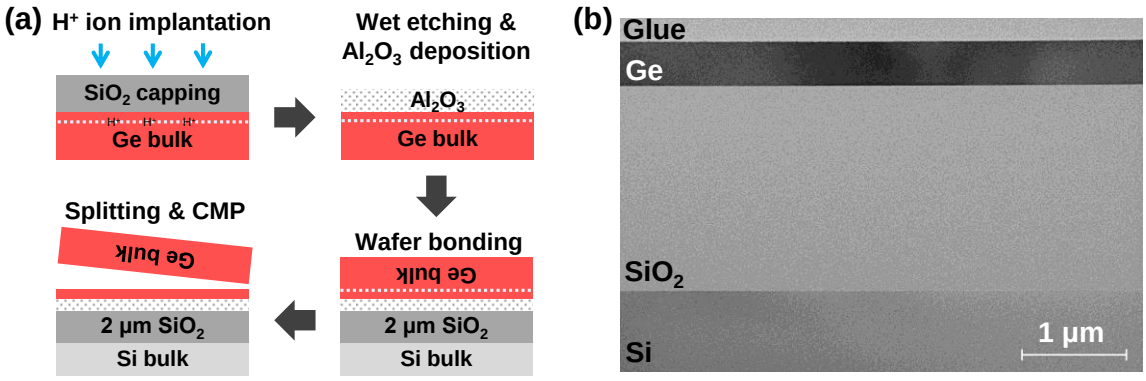

Figure 13. (a) fabrication procedure of GeOI wafer and (b) cross-sectional TEM image of GeOI wafer fabricated by wafer bonding [26].

Fig. 14(a) shows the residual strain in the Ge layer measured by Raman spectroscopy. There is no strain in the Ge layer just after CMP. However, when annealing the GeOI wafer at a temperature higher than 450 °C, we observe the tensile strain of approximately 1%, which might be attributable to the thermal expansion coefficient mismatch between Ge and Si. We find that optimal annealing at 550 °C can annihilate the crystal damage induced in the Ge layer during the GeOI fabrication. As shown in Figs. 14(b) and (c), we achieve the carrier density of less than 10^{16} cm^{-3} and the Hall hole mobility exceeding 2000 cm^2/Vs, close to the original Ge bulk wafer quality.

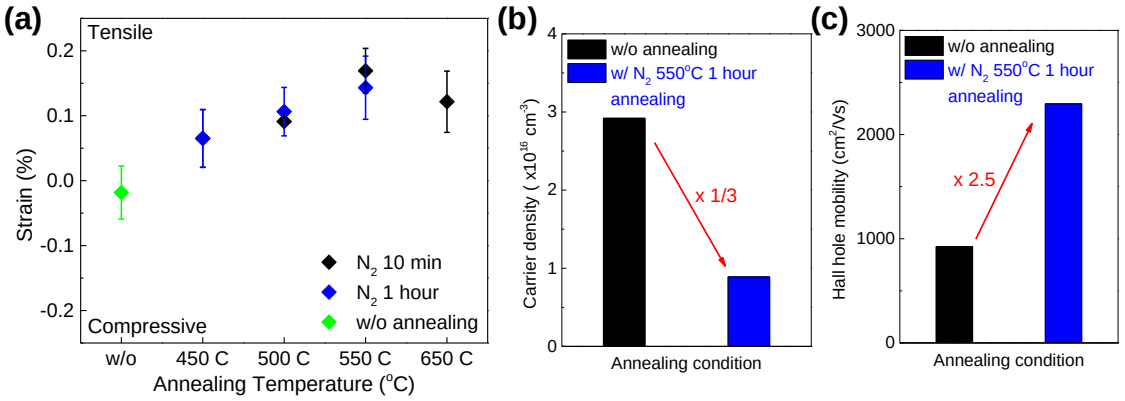

Figure 14. (a) residual strain, (b) carrier density, and (c) Hall hole mobility in the Ge layer of GeOI wafer before and after annealing [26].

By using the wafer bonded GeOI wafer, we have fabricated Ge waveguide as shown in Fig. 15(a) [28]. By using EB lithography and dry etching, a single mode Ge slot waveguide on the GeOI wafer exhibit a good transmission for the 2 μm wavelength band. We have also examined the transmission in the Ge bend waveguide. Since we have the strong optical confinement in the Ge waveguide, we expect there is no significant bend loss. Fig. 15(b) shows the measured bend loss as a function of bending radius. We observe a negligible increase in bend loss even for 5 μm bend radius. Hence, we are able to make ultra-small MIR PICs by using the GeOI platform.

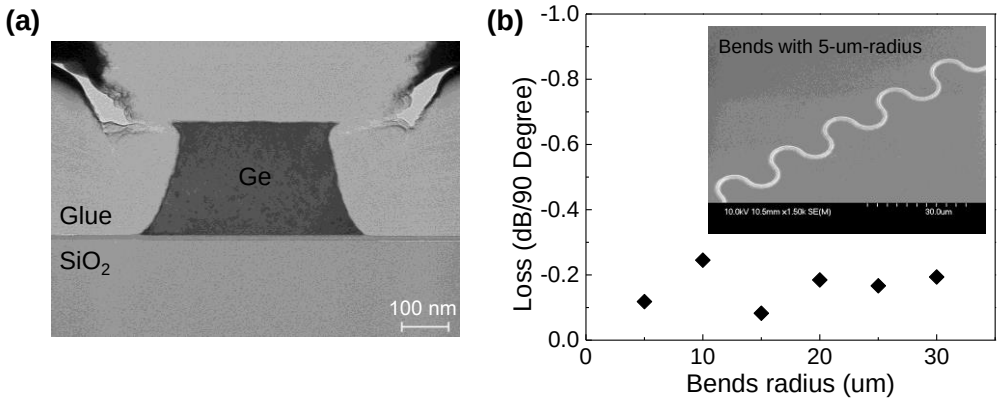

Figure 15. (a) cross-sectional TEM image of Ge strip waveguide on GeOI and (b) bend loss of the Ge waveguide as a function of bend radius [28].

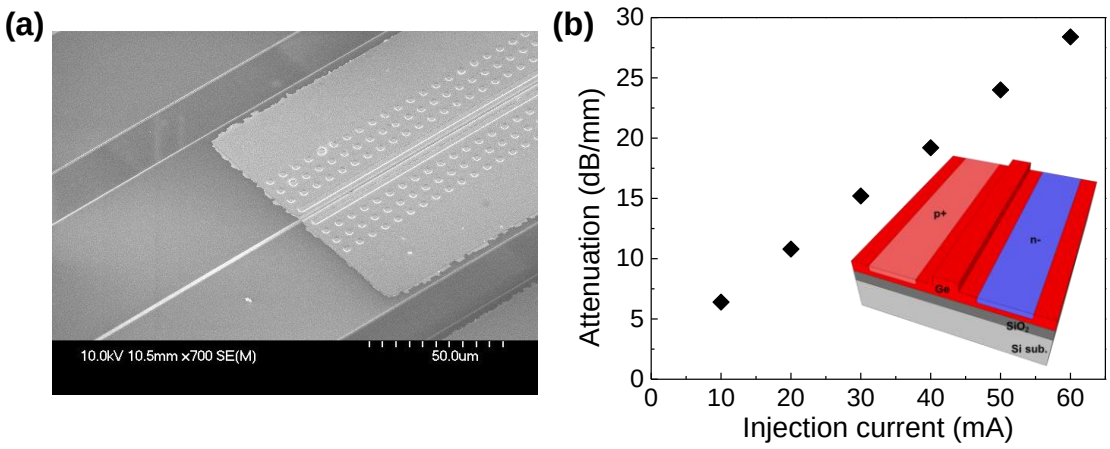

Figure 16. (a) tilted SEM image and (b) attenuation modulation characteristic of carrier-injection Ge optical modulator [28].

Ge is expected to exhibit a factor of ten greater free-carrier absorption than Si at 2 μm wavelength. To examine the absorption modulation by free carriers in Ge, we have fabricated a carrier-injection Ge optical modulator [28]. We form a lateral PIN junction along the Ge waveguide by using ion implantation of B and P. Fig. 16(a) is a tilted SEM image of the device. Fig. 16(b) shows the absorption modulation at a 2 μm wavelength. As shown in Fig. 16(b), we have successfully demonstrated the free-carrier induced absorption modulation in the Ge waveguide at a 2 μm wavelength for the first time. By using the lateral PIN or PN junction, we are able to integrate Ge/GeSn-based lasers and PDs toward Ge-based MIR PICs.

Conclusion

The heterogeneous integration of SiGe and Ge gives us a lot of opportunities to develop photonic integrated circuits for near and mid-infrared wavelengths as well as CMOS-based electronic circuits. We have presented that the strain engineering by strained SiGe is also effective to enhance the modulation efficiency in Si-based optical modulators. Since SiGe is widely used in CMOS fabs, SiGe optical modulators are going to be ready for mass production. In addition to Ge PDs, we have proposed Ge photonics on GeOI platform instead of Si photonics, opening up a frontier of mid-infrared integrated photonics.

Acknowledgments

This work was supported by a Grant-in-Aid for Young Scientists (S) from MEXT, and NEDO “PECST” project.

References

1. S. Gupta, X. Gong, R. Zhang, Y.-C. Yeo, S. Takagi, and K.C. Saraswat, MRS Bull. **39**, 678 (2014).
2. J. A. del Alamo, Nature **479**, 317 (2011).

3. J. Michel, J. Liu, and L.C. Kimerling, Nat. Photonics **4**, 527 (2010).
4. J. Liu, X. Sun, R. Camacho-Aguilera, L.C. Kimerling, and J. Michel, Opt. Lett. **35**, 679 (2010).
5. R.E. Camacho-Aguilera, Y. Cai, N. Patel, J.T. Bessette, M. Romagnoli, L.C. Kimerling, and J. Michel, Opt. Express **20**, 11316 (2012).
6. J. Liu, M. Beals, A. Pomerene, S. Bernardis, R. Sun, J. Cheng, L.C. Kimerling, and J. Michel, Nat. Photonics **2**, 433 (2008).
7. H. H. Tseng, H. Li, V. Mashanov, Y.J. Yang, H.H. Cheng, G.E. Chang, R. a. Soref, and G. Sun, Appl. Phys. Lett. **103**, 231907 (2013).
8. S. Wirths, R. Geiger, N. von den Driesch, G. Mussler, T. Stoica, S. Mantl, Z. Ikonic, M. Luysberg, S. Chiussi, J.M. Hartmann, H. Sigg, J. Faist, D. Buca, and D. Grützmacher, Nat. Photonics **9**, 88 (2015).
9. G. Reed, G. Mashanovich, F. Gardes, and D. Thomson, Nat. Photonics **4**, 518 (2010).
10. R. Soref and B. Bennett, IEEE J. Quantum Electron. **23**, 123 (1987).
11. M. Takenaka and S. Takagi, IEEE J. Quantum Electron. **48**, 8 (2012).
12. Y. Kim, M. Takenaka, T. Osada, M. Hata, and S. Takagi, Sci. Rep. **4**, 4683 (2014).
13. Y. Kim, J. Fujikata, S. Takahashi, M. Takenaka, and S. Takagi, Opt. Express **23**, 12354 (2015).
14. Y. Kim, J. Fujikata, S. Takahashi, M. Takenaka, and S. Takagi, Opt. Express **24**, 1979 (2016).
15. Y. Kim, J. Han, M. Takenaka, and S. Takagi, Opt. Express **22**, 7458 (2014).
16. Y. Kim, M. Takenaka, and S. Takagi, IEEE J. Quantum Electron. **51**, 1 (2015).
17. J. Fujikata, M. Noguchi, Y. Kim, S. Takahashi, T. Nakamura, and M. Takenaka, IEEE Int. Conf. Group IV Photonics **WD2** (2015).
18. J. Han, R. Zhang, T. Osada, M. Hata, M. Takenaka, and S. Takagi, Appl. Phys. Express **6**, 051302 (2013).
19. J. Han, R. Zhang, T. Osada, M. Hata, M. Takenaka, and S. Takagi, Microelectron. Eng. **109**, 266 (2013).
20. M. Takenaka, K. Morii, M. Sugiyama, Y. Nakano, and S. Takagi, Jpn. J. Appl. Phys. **50**, 1 (2011).
21. M. Takenaka, K. Morii, M. Sugiyama, Y. Nakano, and S. Takagi, Opt. Express **20**, 8718 (2012).
22. H. Matsubara, T. Sasada, M. Takenaka, and S. Takagi, Appl. Phys. Lett. **93**, 032104 (2008).
23. J. Kang, R. Zhang, M. Takenaka, and S. Takagi, Opt. Express **23**, 16967 (2015).
24. R. Soref, Nat. Photonics **4**, 495 (2010).
25. R. Soref, Nat. Photonics **9**, 358 (2015).
26. J. Kang, X. Yu, M. Takenaka, and S. Takagi, Mater. Sci. Semicond. Process. **42**, 259 (2015).
27. R. Zhang, T. Iwasaki, N. Taoka, M. Takenaka, and S. Takagi, Appl. Phys. Lett. **98**, 112902 (2011).
28. J. Kang, M. Takenaka, and S. Takagi, Opt. Express **24**, 11855 (2016).